

Refining the airborne wind energy systems power equations with a vortex wake model

Filippo Trevisi¹, Carlo E.D. Riboldi¹, and Alessandro Croce¹

¹Department of Aerospace Science and Technology, Politecnico di Milano, Via La Masa 34, 20156 Milano, Italy

Correspondence: F. Trevisi (filippo.trevisi@polimi.it)

Abstract. The power equations of crosswind Ground-Gen and Fly-Gen airborne wind energy systems (AWESs) flying in circular trajectories are refined to include the contribution from the aerodynamic wake, modelled with vortex methods. This allows to understand reveals the effect of changing turning radius, wing geometry and aerodynamic coefficients on the aerodynamic performances and power production. A novel power coefficient is defined by normalizing the aerodynamic power with the wind power passing through a disc with radius equal to the AWES wing span, allowing to compare different designs for a given wing span. The aspect ratio which maximizes this power coefficient (i.e. which maximizes the aerodynamic power for a given wing span) is finite and its analytical expression for an infinite turning radius is derived. By considering the optimal wing aspect ratio, the maximum power coefficient is found and its analytical expression for an infinite turning radius is derived. Ground-Gen and Fly-Gen AWESs, with the same geometry idealized characteristics, are compared in terms of power production and later three AWESs from the literature are analyzed. With this modeling framework, Ground-Gen systems are found to have lower power potential than the same geometry Fly-Gen AWESs with the same geometry because the reel-out velocity makes them Ground-Gen AWESs to fly closer to their own wake.

1 Introduction

Airborne Wind Energy (AWE) is the field of wind energy in which airborne systems, connected to the ground through a tether, harvest high altitude wind power. Airborne Wind Energy Systems (AWESs) can be classified, based on their flight operations, in as crosswind, rotational and tether aligned (Vermillion et al. (2021)). The mechanical power can be converted into electrical on the ground with a moving or fixed ground station (Ground-Gen) or with onboard wind turbines and transmitted to the ground through the tether (Fly-Gen). In this work, the power equations of ~~concerns~~ Ground-Gen and Fly-Gen crosswind AWESs featuring a single wing are refined.

The first theoretical power equation of crosswind AWESs is derived by Loyd (1980), for given lift and drag coefficients of the system. Other works (e.g. Diehl (2013); Schmehl et al. (2013); Luchsinger (2013); Argatov and Silvennoinen (2013)) follow Loyd's effort and refine the power equation, which is still based on given system aerodynamic coefficients. To use these models, the lift and drag coefficients need then to be known or modelled. In particular, the lift coefficient is typically modelled as function of the wing angle of attack, the wing geometry and the airfoils characteristics. A desired desirable and feasible (i.e. before stall) lift coefficient can be obtained by pitching the wing to obtain the correspondent corresponding angle of attack.

The system drag coefficient include contributions from the ~~viseous and pressure~~ wing profile drag, the tether drag (Trevisi et al. (2020a)), ~~and~~ the induced drag ~~and the drag of all AWES components excluding the wing and the tether~~. The ~~latter~~ induced drag is the result of the velocities induced by the AWES ~~wake trailed vorticity (wake)~~ on the AWES wing itself. ~~Indeed, the finite AWES wing trails vortices according to the span-wise lift distribution~~. The ~~indueed~~ velocities induced by the trailed vortices reduce the relative wind velocity ~~intensity magnitude~~ and effectively rotate the ~~relative apparent~~ velocity, composed by the undisturbed relative wind velocity and the AWES velocity, of an induced angle. Since the aerodynamic lift is defined to be perpendicular to the local ~~relative apparent~~ velocity, it is rotated by the induced angle. The component of lift parallel to the undisturbed ~~relative apparent~~ velocity is then the induced drag. In AWE, the induced velocities and the induced drag are typically estimated using Prandtl lifting-line theory, developed for wings in forward flight (i.e. the aerodynamic wake is straight). For example, Vander Lind (2013); Bauer et al. (2018) and Trevisi et al. (2020b) refine Loyd power equation by finding the induced drag coefficient with the straight wake assumption. To overcome the straight wake assumption in engineering models, the induced velocities are modelled with momentum methods (De Lellis et al. (2018); Kheiri et al. (2018, 2019)) and vortex methods (Leuthold et al. (2019); Gaunaa et al. (2020); Trevisi et al. (2023b)).

Gaunaa et al. (2020) point out that using momentum methods to analyze the induction for an AWES, which is described by 3D polars, is not physically consistent. Indeed, momentum theory is used in rotor aerodynamics to find the velocity triangle of an airfoil (2D polars) along the blade. If then momentum theory is used to evaluate the induction at an airfoil in the AWES wing (2D polars), a root and a tip correction would be needed to take into account that the rotor is not a disc, but a single wing. However, the corrections for AWESs would differ largely from wind turbines corrections, as these are developed for blades extending almost to the rotation axis, and need a dedicated study. Gaunaa et al. (2020) then introduce a vortex-based engineering model to find the induced velocities at the AWES. Based on these considerations, Trevisi et al. (2023b) find an induced drag coefficient of the AWES with vortex methods. The helicoidal wake structure is modelled with an expression for the near wake (first half rotation of the wake) and one for the far wake (from the second half of the wake to infinity). The induced drag related to the near wake is found to be similar to the induced drag the same wing would have in forward flight (i.e. with straight wakes). The induced drag coefficient related to the far wake is modelled as function of the near wake drag coefficient, the ratio between the wing span and the turning radius and the helicoidal wake pitch. The ~~latter helicoidal wake pitch~~ can be found iteratively as function of the other geometrical and aerodynamic quantities. The model is validated with the the lifting line free vortex wake method (Marten et al. (2015)) implemented in QBlade.

In this work, a power equation refinement, based on the aerodynamic modelling from Trevisi et al. (2023b), is introduced ~~and a novel power coefficient is defined~~. Properly including the aerodynamic wake into the power equation ~~allows to understand~~ reveals the effect of changing turning radius, wing aspect ratio and aerodynamic coefficients on the overall performance. ~~The novel power coefficient allows to compare different concepts and define optimal geometrical quantities~~. This work is particularly relevant when studying the performance of a given system or carrying out a system design study.

This paper is organized as follows: In Sect. 2, the main assumptions and equations of the vortex model from Trevisi et al. (2023b) are recalled, to make this manuscript self-contained. In Sect. 3 and 4, the power equations of Ground-Gen and Fly-Gen AWESs are derived. In Sect. 5, Ground-Gen and Fly-Gen AWESs, with the same geometry, are compared in terms of power

production. In Sect. 6, three AWES designs from the literature are analyzed. In Sect. 7, the main conclusions are discussed. A nomenclature is given in Appendix A.

2 Vortex wake model

In this section, the main assumptions and final equations of the vortex wake model introduced by Trevisi et al. (2023b) are summarized. The velocities induced at the AWES from the helicoidal trailed vortex filaments are modeled with an expression for the near wake and one for the far wake. The near wake is modeled as the first half rotation of the helicoidal filaments, with their axial component being neglected. The far wake is modeled as two semi-infinite vortex ring cascades with opposite intensity. This model is employed to refine the Ground-Gen and Fly-Gen AWES power equations in the next sections.

Referring to Fig. 1, the AWES moves on a circular trajectory with radius R_0 in the plane (e_1, e_2) , which is perpendicular to the incoming wind $v_w = -v_w e_3$. In this model, the wind is assumed constant and the gravity is neglected. The AWES has a constant speed and its wing, assumed to be elliptical, is on the rotational plane. Trevisi et al. (2022a) show that these are the optimal trajectories for a Fly-Gen maximising thrust power with constant inflow and the AWES flight mechanics can be studied about this condition (Trevisi et al. (2021)). For Ground-Gen AWESs, the inertial reference frame (e_1, e_2, e_3) moves with the reel-out velocity of the tether is $v_o = -v_o e_3$, assumed to be only along the axial direction, such that the relative wind velocity is $v_r = v_w - v_o$. For Fly-Gen AWESs, the tether and the inertial reference frame are fixed and the relative wind velocity coincides with the wind velocity $v_r = v_w$.

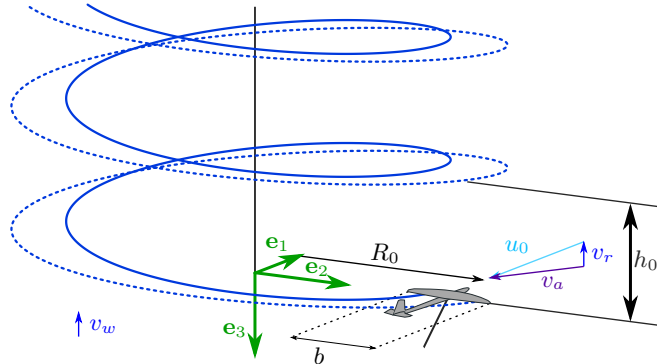


Figure 1. Wake structure of an AWES flying circular trajectories. The solid and dashed blue lines represent the left and right rolled up vortices respectively.

The wake, assumed to be non expanding, is transported downwind by the wind and has a helicoidal shape. The wake model is divided into an expression for the near wake, which is defined as the first half rotation of the wake, and one for the far wake, which is from the second half rotation to infinity.

80 The induced drag coefficient due to the near wake is similar to the induced drag coefficient the same wing would have in forward flight

$$C_{Di}^n \approx \frac{C_L^2}{\pi AR}, \quad (1)$$

where C_L and AR are the wing lift coefficient and the aspect ratio, respectively.

The induced drag coefficient due to the far wake is

85
$$C_{Di}^f \approx \frac{1}{4\pi} \frac{C_L^2}{\pi AR} \kappa_0^{\pi/2} \lambda_0^{3/2}, \quad (2)$$

where $\kappa_0 = \frac{b}{2R_0}$ is the inverse turning ratio, defined as the ratio between the half-span $b/2$ and the turning radius R_0

$$\kappa_0 = \frac{b}{2R_0}, \quad (3)$$

and λ_0 is the normalized torsional parameter of the helicoidal wake, which physically represents the ratio between the circumference length, which is known, and the helix pitch h_0 , which is unknown,

90
$$\lambda_0 = \frac{2\pi R_0}{h_0}. \quad (4)$$

The system aerodynamic drag coefficient C_D is the sum of the parasite drag coefficient $C_{D,p}$ (Anderson (2017)) and the induced drag coefficient C_{Di}

$$C_D = \underbrace{C_d + C_{D,c} + C_{D,t}}_{C_{D,p}} + \underbrace{C_{Di}^n + C_{Di}^f}_{C_{Di}}. \quad (5)$$

C_d is the wing profile drag. $C_{D,c}$ contains the drag of the tail surfaces, fuselage, turbines nacelles (if present), and any other component of the AWES exposed to the airflow excluding the tether. $C_{D,t} = C_{D\perp} \frac{D_t L_t}{4A}$ is the equivalent tether drag, with $C_{D\perp}$ being the drag coefficient of the tether section, D_t the tether diameter, L_t the tether length and A the main wing area (Trevisi et al. (2020a)).

95

Considering the drag coefficient related to the near and far wake, The system glide ratio is

$$G = \frac{C_L}{C_D + C_{T,t}} = \frac{C_L}{C_{D,p} + \frac{C_L^2}{\pi AR} + \frac{1}{4\pi} \frac{C_L^2}{\pi AR} \kappa_0^{\pi/2} \lambda_0^{3/2} + C_{T,t}}, \quad (6)$$

100 where ~~C_D is the system aerodynamic drag, $C_{D,p}$ is the system drag coefficient at zero lift and $C_{T,t}$ is a coefficient modelling the thrust of the onboard wind turbines, in case of Fly-Gen AWESs. More details on $C_{T,t}$ are given in Sect. 4. $C_{D,p}$ is the summation of the aircraft viscous and pressure drag $C_{D,v}$ and the equivalent tether drag $C_{D,t} = C_{D\perp} \frac{D_t L_t}{4A}$, where $C_{D\perp}$ is the drag coefficient of the tether section, D_t the tether diameter, L_t the tether length and A the main wing area.~~

The axial velocity of the vortex filaments, needed to find the helix pitch h_0 (Eq. 4), is assumed to be equal to the wind velocity minus the velocity induced by the near wake, so that

105

$$\lambda_0 = \frac{1}{\frac{1}{\lambda} - \frac{C_L}{\pi AR}}, \quad (7)$$

where the wing speed ratio $\lambda = \frac{u_0}{v_r}$ is defined as the ratio between the AWES tangential velocity u_0 and the relative wind speed v_r . For the AWES to have a constant speed, the lift, perpendicular to the apparent velocity v_a , combines with the drag, parallel to v_a , such that the force balance along the AWES longitudinal direction e_1 is null. The wing speed ratio $\lambda = \frac{u_0}{v_r}$ needs to be equal to the glide ratio G (see Fig. 2 for Ground-Gen and Fig. 4 for Fly-Gen AWESs).

$$\lambda = G. \quad (8)$$

The normalized torsional parameter λ_0 , necessary for the evaluation of the far-wake induced drag due to the far wake C_{Di}^f (Eq. 2), can be found with

$$\lambda_0 = \frac{\lambda}{\sqrt{(1-a_z)^2 + a_r^2}}, \quad (9)$$

where a_z is the axial induction

$$a_z = \lambda \frac{C_L}{\pi AR} \left(1 + \frac{1}{4\pi} \kappa_0^{\pi/2} \lambda_0^{3/2} \right), \quad (10)$$

and a_r the radial induction

$$a_r = \lambda \frac{2}{9\pi} \frac{C_L}{\pi AR} \kappa_0^{\pi/2} \lambda_0^{1.1}. \quad (11)$$

The normalized torsional parameter λ_0 can be found numerically by setting the residual h of Eq. (7) to zero

$$h(\lambda_0, C_{D,p}, C_{T,t}, C_L, AR, \kappa_0) = \lambda_0 - \frac{\lambda}{\sqrt{(1-a_z)^2 + a_r^2}} \frac{1}{\frac{1}{\lambda} - \frac{C_L}{\pi AR}} = 0, \quad (12)$$

where a_z and a_r are given in Eqs. (10) and (11), the wing speed ratio λ is equal to the glide ratio G , which is given in Eq. (6).

3 Reel-out power equation of Ground-Gen AWESs

In this section, the power equation of Ground-Gen AWESs, considering the helicoidal wake modelling given in Sect. 2, is derived.

Referring to Fig. 2, the relative wind velocity $v_r = v_w - v_o$ is the difference between the incoming wind velocity v_w and the axial component of the reel-out velocity $v_r = v_w - v_o$. In accordance with the vortex wake model of Sect. 2, the incoming wind is assumed constant and the gravity is neglected, which makes the problem axial-symmetric. In steady state, the forces acting on the AWES need to be in equilibrium. For the force balance along e_1 to be null, the lift, perpendicular to the apparent velocity v_a , combine with the drag, parallel to the apparent velocity, such that the force balance along the AWES longitudinal direction e_1 is null. The wing speed ratio $\lambda = u_0/v_r$ needs to be equal to the glide ratio G . For the force balance along e_3 to be null, the axial component of the tensile force acting on the tether T_{GG} needs to be equal to the total aerodynamic force

$$T_{GG} = \sqrt{L^2 + D^2} = \frac{1}{2} \rho A C_L v_a^2 \sqrt{1 + \frac{1}{G^2}}, \quad (13)$$

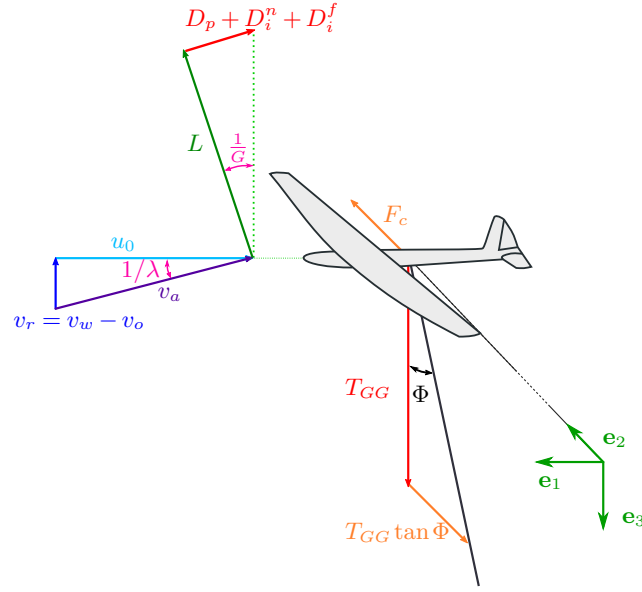


Figure 2. Velocity triangle and forces acting on a Ground-Gen AWES in crosswind steady state.

where ρ is the air density, A is the wing area and $v_a = \sqrt{u_0^2 + v_r^2} = u_0 \sqrt{1 + \frac{1}{\lambda^2}}$ is the apparent velocity, and can be approximated, for high glide ratios, with the lift force generated by the AWES flying at the velocity $u_0 = G v_r$. For high glide ratios G (and thus high wing speed ratio λ), T_{GG} can be then approximated with

$$T_{GG} \approx \frac{1}{2} \rho A C_L G^2 v_w^2 (1 - \gamma_o)^2, \quad (14)$$

where ρ is the air density, A is the wing area and $\gamma_o = \frac{v_o}{v_w}$ is the reel-out factor (measuring how much the tether is reeled out along the axial direction with respect to the wind speed).

For Looking at the force balance along e_2 to be null, if the centrifugal force $F_c = m \frac{u_0^2}{R_0}$, where with m is being the AWES mass plus one third of the tether mass (Trevisi et al. (2020a)) and $R_0 = L_t \sin \Phi$, needs to be equal to the radial component of the tether force $T_{GG} \tan \Phi$, then the lift is entirely used for power production. This condition is obtained by choosing the opening angle Φ of the cone swept by the tether over the loop which satisfies (Trevisi et al. (2020a))

$$\sin \Phi \tan \Phi = \frac{m}{\frac{1}{2} \rho C_L A L_t}. \quad (15)$$

The reel-out power is then the product between the axial component of the tether force T_{GG} and the axial component of the reel-out velocity $v_o = v_w \gamma_o$

$$P_{GG} = \frac{1}{2} \rho A C_L G^2 v_w^3 \gamma_o (1 - \gamma_o)^2. \quad (16)$$

Taking inspiration from conventional wind energy, a power coefficient can be obtained by normalizing the power P_{GG} with a reference kinetic energy per unit time, i.e. the power of the flow passing through a reference area A_{ref} . In the case of

conventional wind turbines, this reference kinetic energy rate is commonly defined by the far field flow velocity value and the rotor disc area. In AWE, one could take as a reference area the annulus swept by the AWES $A_{ref} = 2\pi R_0 b$ (blue area in Fig. 3). However, this area varies at different wind speeds as the turning radius R_0 depends on the AWES lift coefficient C_L through Eq. (15) (note that $R_0 = L_t \sin \Phi$). A second option would be to take as reference area the AWES wing area $A_{ref} = A$. This would lead to the power harvesting factor PHF , as defined by Diehl (2013) and Kheiri et al. (2019). The power harvesting factor allows to compare AWESs for a given wing area. A third option, used in this work, is to take A_{ref} as the area of a disc with radius equal to the AWES wing span $A_{ref} = \pi b^2$ (orange area in Fig. 3). With this definition, A_{ref} is a fixed value defined by the geometry of the system, as for conventional wind turbines, and allows to compare AWESs for a given wing span. Moreover, A_{ref} is the reference area of an equivalent conventional turbine characterized by the same lifting body span (i.e. the wind turbine blades and the AWES wing have the same span). The advantage of this power coefficient definition compared to the first two will be evident when analyzing the results in Sect. 5. Adopting the latter reference area definition and writing the wing area as $A = \frac{b^2}{AR}$, the power coefficient is

$$C_{P,GG} = \frac{P_{GG}}{\frac{1}{2}\rho v_w^3 A_{ref}} = \gamma_o(1 - \gamma_o)^2 \frac{C_L}{\pi AR} \left(\frac{C_L}{C_D} \right)^2. \quad (17)$$

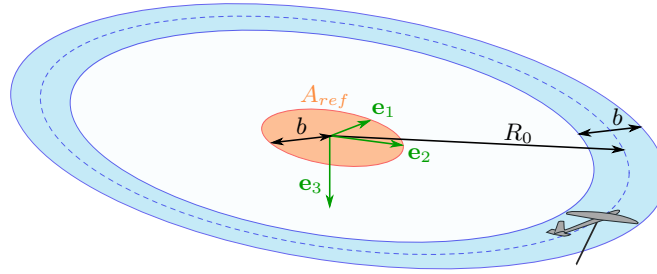


Figure 3. Reference area for the power coefficient evaluation.

With the same approach, a thrust coefficient can be defined as

$$C_{T,GG} = \frac{T_{GG}}{\frac{1}{2}\rho v_w^2 A_{ref}} = (1 - \gamma_o)^2 \frac{C_L}{\pi AR} \left(\frac{C_L}{C_D} \right)^2. \quad (18)$$

The ratio between the power and the thrust coefficient is then

$$\frac{C_{P,GG}}{C_{T,GG}} = \gamma_o. \quad (19)$$

Since the system drag coefficient is not influenced by the relative wind speed at the AWES, $C_{P,GG}$ is maximized when the term $\gamma_o(1 - \gamma_o)^2$ is maximized, which is for $\gamma_o = 1/3$. The maximum power coefficient is then

$$C_{P,GG}^* = \frac{4}{27} \frac{C_L}{\pi AR} \left(\frac{C_L}{C_D} \right)^2. \quad (20)$$

Note that this power coefficient does not model the reel-in phase and the power losses due to the potential energy exchange.

In this section, the power equation of Fly-Gen AWESs, considering the wake model given in Sect. 2, is derived.

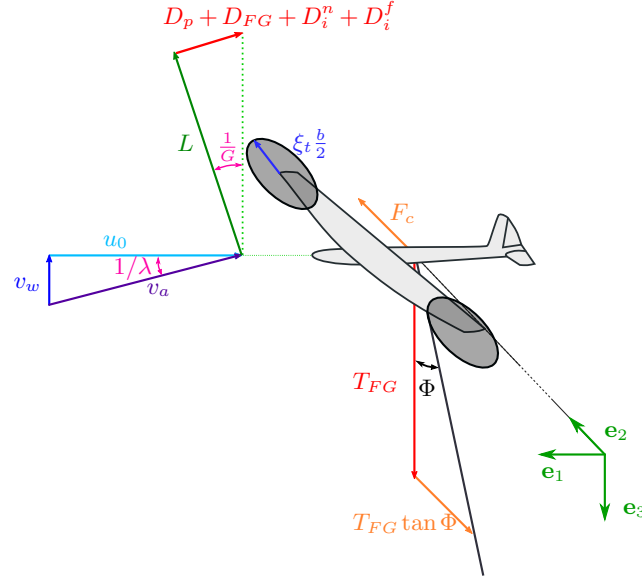


Figure 4. Velocity triangle and forces acting on a Fly-Gen AWES in crosswind steady state.

For a Fly-Gen, as no reel-out velocity is present, the relative wind speed is the actual wind speed $v_r = v_w$. The incoming wind is assumed constant and gravity is neglected in this work, such that the problem is axial-symmetric. In steady state, the forces acting on the AWES need to be in equilibrium. For the force balance along e_1 to be null, the lift, perpendicular to the apparent velocity v_a , combines with the drag, parallel to v_a , such that the force balance along the AWES longitudinal direction e_1 is null. The wing speed ratio $\lambda = u_0/v_r$ needs to be is then equal to the glide ratio G . For the force balance along e_3 to be null, the axial component of the tensile force acting on the tether T_{FG} needs to be equal to the total aerodynamic force $L\sqrt{1 + \frac{1}{G^2}}$. and can be approximated, for high glide ratios, with the lift force generated by the AWES flying at the velocity $u_0 = G v_w$. For high glide ratios G (and thus high wing speed ratio λ), T_{FG} can be approximated with the aerodynamic lift L and the apparent velocity $v_a = u_0\sqrt{1 + \frac{1}{\lambda^2}}$ can be approximated with the longitudinal velocity $u_0 = G v_w$. T_{FG} becomes

$$T_{FG} \approx \frac{1}{2} \rho A C_L G^2 v_w^2. \quad (21)$$

For the force balance along e_2 to be null without contributions from the lift, Eq. (15) needs to be satisfied, as for Ground-Gen AWESs.

Assuming that the onboard turbines rotors are perpendicular to the AWES motion, the thrust force produced by the onboard wind turbines is

$$D_{FG} = \frac{1}{2} \rho A C_{T,t} G^2 v_w^2, \quad (22)$$

where $C_{T,t}$ is the thrust coefficient of the onboard wind turbines with respect to the wing area (and not to the onboard wind turbines rotor area, as typically done for conventional wind energy). As D_{FG} is felt by the AWES dynamics as a drag force, $C_{T,t}$ should be included into the system glide ratio estimation, as in Eq. (6). $C_{T,t}$ can be expressed as function of the aerodynamic drag as $C_{T,t} = \gamma_t C_D$, where C_D is the system drag. γ_t is then the ratio between the onboard wind turbine thrust and the aerodynamic system drag. The system glide ratio is then

$$G = \frac{C_L}{\left(C_{D,p} + \frac{C_L^2}{\pi AR} + \frac{1}{4\pi} \frac{C_L^2}{\pi AR} \kappa_0^{\pi/2} \lambda_0^{3/2} \right) (1 + \gamma_t)}. \quad (23)$$

The thrust power of the onboard wind turbines $P_{t,FG}$ is the product between the thrust force D_{FG} and the Fly-Gen AWES velocity $u_0 = Gv_w$

$$P_{t,FG} = \frac{1}{2} \rho A \gamma_t C_D G^3 v_w^3. \quad (24)$$

The shaft power of the onboard wind turbines P_{FG} (i.e., the mechanical power that can be converted to electrical power) is modeled using 1D momentum theory (actuator disc). The onboard wind turbine thrust (Eq. 22) can be formulated with momentum theory

$$D_{FG} = \frac{1}{2} \rho A_t (4a_t(1 - a_t)) G^2 v_w^2 \approx \frac{1}{2} \rho A_t (4a_t) G^2 v_w^2, \quad (25)$$

where A_t is the total turbines area and the onboard wind turbines induction a_t is assumed small. By setting equal Eqs. (22) and (25), the onboard wind turbines induction is $a_t = \frac{\gamma_t C_D}{4} \frac{A}{A_t}$ and the shaft power is

$$P_{FG} = (1 - a_t) P_{t,FG} \approx \left(1 - \frac{\gamma_t C_D}{4} \frac{A}{A_t} \right) P_{t,FG}. \quad (26)$$

~~where the onboard wind turbines induction a_t , assumed small, is found by setting Eq. (22) equal to the thrust given by momentum theory $D_{FG} = \frac{1}{2} \rho A_t (4a_t(1 - a_t)) G^2 v_w^2 \approx \frac{1}{2} \rho A_t (4a_t) G^2 v_w^2$ (Trevisi et al. (2020b)) and A_t is the total turbines area.~~ A small value of $a_t \approx \frac{\gamma_t C_D}{4} \frac{A}{A_t}$ is necessary to reduce power losses due to the onboard wind turbines induction and to the potential energy exchange (Trevisi et al. (2022a)). The turbines radius can be expressed as a function of the wing span as $R_t = \xi_t \frac{b}{2}$ (Fig. 4). The total rotor area of the turbines is $A_t = n_t \frac{\pi}{4} \xi_t^2 b^2$, where n_t is the number of turbines, assumed to be all of the same size. To present results in a more concise way, without losing generality, the number of turbines is assumed to be equal to two $n_t = 2$, such that $\xi_t \in [0, 1]^1$. The shaft power can be written as

$$P_{FG} = \frac{1}{2} \rho A \gamma_t C_D G^3 v_w^3 \left(1 - \frac{\gamma_t C_D}{2\pi AR \xi_t^2} \right). \quad (27)$$

The thrust power coefficient of Fly-Gen AWES, taking the reference area as the disc with radius equal to the AWES wing span, is

$$C_{P_{t,FG}} = \frac{P_{t,FG}}{\frac{1}{2} \rho v_w^3 A_{ref}} = \frac{\gamma_t}{(1 + \gamma_t)^3} \frac{C_L}{\pi AR} \left(\frac{C_L}{C_D} \right)^2, \quad (28)$$

¹The limiting case with $\xi_t = 1$ can be obtained with the two turbines placed at the wing tips. This corresponds to the largest value of A_t possible, considering $n_t \geq 2$.

where C_D depends on γ_t through the **far wake induced drag (the normalized torsional parameter λ_0 is function of λ , which is function of γ_t)**. In the case of straight wakes ($\kappa_0 = 0$) the optimal value of γ_t which maximize the thrust power $P_{t,FG}$ is $\gamma_t = 1/2$ (Loyd (1980)). Using this value, the thrust power coefficient is

$$C_{P_{t,FG}} \left(\gamma_t = \frac{1}{2} \right) = \frac{4}{27} \frac{C_L}{\pi AR} \left(\frac{C_L}{C_D} \right)^2, \quad (29)$$

which coincides with the maximum power coefficient of Ground-Gen AWESs when $\kappa_0 = 0$: $C_{P_{t,FG}}(\gamma_t = 1/2, \kappa_0 = 0) = C_{P_{t,GG}}^*(\kappa_0 = 0)$ (Eq. 20). For κ_0 larger than zero, the far wake contributes in different ways for the two generation types, leading to different power coefficient. This is shown in Sect. 5.

The shaft power coefficient includes power losses due to the onboard wind turbines induction

$$C_{P_{t,FG}} = \frac{P_{FG}}{\frac{1}{2} \rho v_w^3 A_{ref}} = \frac{\gamma_t}{(1 + \gamma_t)^3} \frac{C_L}{\pi AR} \left(\frac{C_L}{C_D} \right)^2 \left(1 - \frac{\gamma_t C_D}{2\pi AR \xi_t^2} \right). \quad (30)$$

Note that this power coefficient does not model power losses due to the potential energy exchange. See Trevisi et al. (2022a) for more details on these losses.

With the same approach, The thrust coefficient can be defined as

$$C_{T_{t,FG}} = \frac{T_{FG}}{\frac{1}{2} \rho v_w^2 A_{ref}} = \frac{1}{(1 + \gamma_t)^2} \frac{C_L}{\pi AR} \left(\frac{C_L}{C_D} \right)^2. \quad (31)$$

and ratio between power and thrust coefficient is

$$\frac{C_{P_{t,FG}}}{C_{T_{t,FG}}} = \frac{\gamma_t}{1 + \gamma_t} \left(1 - \frac{\gamma_t C_D}{2\pi AR \xi_t^2} \right). \quad (32)$$

5 Comparison between Ground-Gen and Fly-Gen AWESs

In this section, Ground-Gen and Fly-Gen AWES performances are compared according to the mathematical models introduced in the previous sections. **As a given design can be operated at lift coefficients different from the lift coefficient the AWES is designed for, the analyses are initially performed as function of the operational AWES lift coefficient C_L . Later in the section, the design lift coefficient \tilde{C}_L is considered as the varying parameter to study its influence of the geometrical design and on the performances.**

The first study concerns Fly-Gen AWESs and addresses the effects of the parameter ξ_t , which indicates the size of the onboard wind turbines (Fig. 4), on their aerodynamic induction a_t . **First, a parametric study for Fly-Gen on the parameter ξ_t , which indicates the size of the onboard wind turbines (Fig. 4), is carried out.** A case with $AR = 20$, $C_{D,p} = 0.05$ and the inverse turning ratio $\kappa_0 = \frac{b}{2R_0} = 0.15$ is considered in this section, corresponding to the example in Trevisi et al. (2023b). Figure 5 shows the optimal values of **the on-board wind turbine thrust factor γ_t** on the left axis and the efficiency due to the onboard wind turbine induction $1 - a_t$ on the right axis, as function of the lift coefficient, for three different ξ_t . The optimal

values of γ_t are found by solving the optimization problem

$$(\gamma_t, \lambda_0)^* = \arg \left(\max_{(\gamma_t, \lambda_0)} C_{P,FG}(\gamma_t, \lambda_0, C_L, C_{D,p}, AR, \kappa_0, \xi_t) \right), \quad (33)$$

subject to: $h(\gamma_t, \lambda_0, C_L, C_{D,p}, AR, \kappa_0) = 0$,

where h is defined in Eq. (12). For low lift coefficients, the optimal value of γ_t is close to 0.5. As soon as the effect of the far wake starts to contribute to the overall drag, γ_t rises slightly above 0.5 to decrease the glide ratio G (Eq. 23) and consequently the normalized torsional parameter λ_0 . Decreasing λ_0 increases the vortex rings axial distance h_0 (Eq. 4) and thus decreases the induction due to the far wake. As expected, smaller onboard turbines decrease the efficiency $1 - a_t$. For the following analyses in this section, it is assumed $\xi_t = 0.15$ when the case with $AR = 20$, $\kappa_0 = 0.15$, $C_{D,p} = 0.05$ is considered, as this is considered a reasonable value.

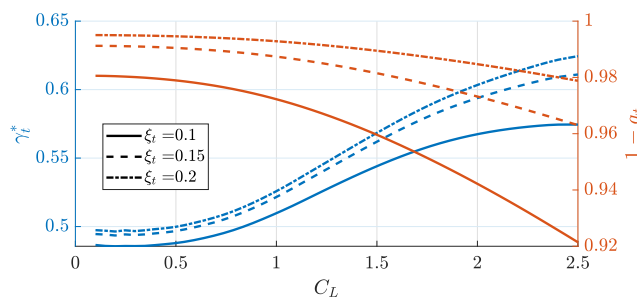


Figure 5. Optimal value of γ_t (blue - left axis) and efficiency due to onboard wind turbine induction (red - right axis) for different onboard wind turbine ~~adimensional~~ non-dimensional radius ξ_t as function of the operational AWES lift coefficient. Case with $AR = 20$, $\kappa_0 = 0.15$, $C_{D,p} = 0.05$.

The second study investigates the difference in normalized torsional parameter and in glide ratio for Ground-Gen and Fly-Gen AWESs, shown in Figure 6. ~~shows the normalized torsional parameters and the glide ratios of Ground-Gen and Fly-Gen AWESs (blue and red line respectively).~~ Ground-Gen values are found by considering the reel-out factor $\gamma_o = 1/3$ and solving numerically Eq. (12). Fly-Gen values are found by solving the optimization problem (33). As the onboard wind turbines thrust is acting as a drag force on Fly-Gen AWESs, they have lower system glide ratio compared to Ground-Gen. The normalized torsional parameter λ_0 informs about the pitch of helicoidal aerodynamic wake and is linked to the wind speed ratio λ , which is equal to the glide ratio $\lambda = G$. ~~(Eq. 8). Since Ground-Gen AWESs have larger glide ratios, they also have larger values of λ_0 compared to Fly-Gen.~~ Larger λ_0 means lower pitches h_0 of the helicoidal aerodynamic wake, according to Eq. (4), and thus higher induced velocities due to the far wake. This is due to the reel-out velocity of Ground-Gen AWES, which make them ~~to~~ fly closer to their own wake.

The third study compares the power coefficient of Ground-Gen and Fly-Gen AWESs for varying aspect ratios as function of the operational lift coefficient and investigate which aspect ratio is optimal as function of the design lift coefficient. Figure 7 shows the optimal power coefficients for Ground-Gen and Fly-Gen AWESs as function of the operational lift coefficient

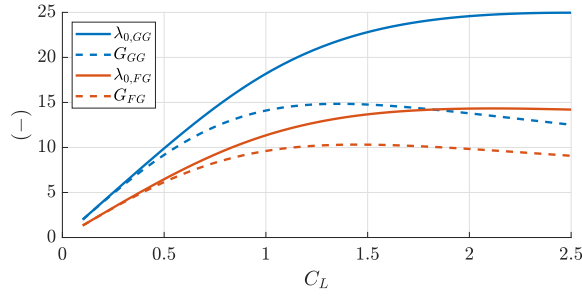


Figure 6. Normalized torsional parameter for a Ground-Gen and a Fly-Gen AWES (solid blue and red line respectively) and glide ratio (dashed blue and red line respectively) as function of the operational lift coefficient. Case with $AR = 20$, $\kappa_0 = 0.15$, $C_{D,p} = 0.05$ and $\xi_t = 0.15$.

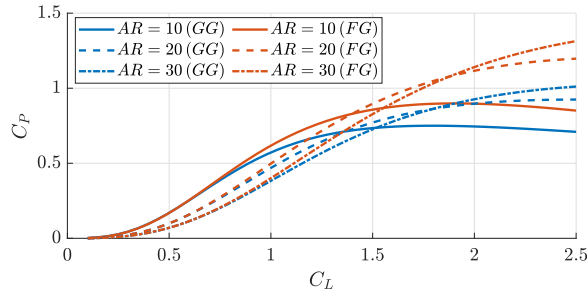


Figure 7. Power coefficients of Ground-Gen (blue lines) and Fly-Gen (red lines) AWESs as function of the operational lift coefficient. Case with $\kappa_0 = 0.15$, $C_{D,p} = 0.05$, $\xi_t = 0.15$ and three different AR values.

for three different aspect ratios. Fly-Gen can extract more aerodynamic power compared to the same geometry Ground-Gen AWESs, due to the far wake pitch. This is in accordance with the findings from Kheiri et al. (2019). Indeed, as discussed when analyzing Fig. 6, Ground-Gen AWESs fly closer to their own wake due to reel-out velocity. Higher power coefficients can be obtained with higher aspect ratios at high operational lift coefficients. In this comparison, if the aspect ratio is doubled (e.g. from 10 to 20), the wing area is halved, as the inverse turning ratio κ_0 (and thus b) is kept constant. To find which aspect ratio maximizes the power coefficient, one could set the partial derivative of C_P with respect to the aspect ratio to zero. The resultant aspect ratio can be then considered in the conceptual design phase of an AWES project. To get to an analytical solution, the wake is considered straight ($\kappa_0 = 0$). The maximum power coefficient for Ground-Gen AWESs ($\gamma_o = 1/3$, Eq. 20) and the thrust power coefficient with $\gamma_t = 1/2$ is considered for Fly-Gen (Eq. 29) are considered. Under these assumptions, the power coefficient of Ground-Gen and Fly-Gen AWESs coincide $C_{P_t,FG}(\gamma_t = 1/2, \kappa_0 = 0) = C_{P,GG}(\gamma_o = 1/3, \kappa_0 = 0)$ (Eqs. 20 and 29). The partial derivative of C_P with respect to the aspect ratio is

$$\frac{\partial C_P}{\partial AR} = \frac{4}{27} \frac{\tilde{C}_L^3}{\pi} \left(\frac{\partial(1/AR)}{\partial AR} \frac{1}{C_D^2} + \frac{1}{AR} \frac{\partial(1/C_D^2)}{\partial AR} \right) = 0, \quad (34)$$

where \tilde{C}_L is the lift coefficient chosen for the design of the aspect ratio and

$$275 \quad \frac{\partial C_D}{\partial AR} = -\frac{1}{AR} C_{Di}^n. \quad (35)$$

After a few steps, the condition which maximizes C_P is found when the induced drag coefficient equals the parasite drag coefficient at zero lift, $C_{Di}^n = C_{D,p}$, which results in

$$AR^\otimes = \frac{1}{\pi} \frac{\tilde{C}_L^2}{C_{D,p}}, \quad (36)$$

with $G_0 = \frac{C_L}{C_{D,p}}$ and where the symbol \otimes indicates an optimal quantity, obtained with analytical models. This aspect ratio answers to the question: "Given a wing span, which is the aspect ratio that maximizes power?". Note that this derivation would not have been possible if the power coefficient was defined as the power harvesting factor PHF (taking as reference area A_{ref} in Eqs. (17) and (28) the wing area A). Indeed, by taking $\frac{\partial PHF}{\partial AR} = 0$, one looks for the aspect ratio which answers to the question: "Given a wing area, which is the aspect ratio that maximize power?". The solution, in this case, to this question is an infinite aspect ratio. This highlights one of the benefits of using a reference area for the power coefficient proportional to the wing span and not to the wing area.

The aspect ratios which maximize the C_P for Ground-Gen and Fly-Gen AWESs, considering the wake structure and the onboard wind turbines induction, can be found by solving two optimization problems.

For Ground-Gen AWESs, the optimal values of γ_o and AR can be found by solving the optimization problem

$$(\gamma_o, AR, \lambda_0)^* = \arg \left(\max_{(\gamma_o, AR, \lambda_0)} C_{P,GG}(\gamma_o, \lambda_0, \tilde{C}_L, C_{D,p}, AR, \kappa_0) \right) \quad (37)$$

subject to: $h(\lambda_0, \tilde{C}_L, C_{D,p}, AR, \kappa_0) = 0$,

290 where h is defined in Eq. (12) and it does not depend on γ_o . Its optimal value is always $\gamma_o^* = 1/3$ (Eq. 20).

For Fly-Gen AWESs, the optimal values of γ_t and AR can be found by solving the optimization problem

$$(\gamma_t, AR, \lambda_0)^* = \arg \left(\max_{(\gamma_t, AR, \lambda_0)} C_{P,FG}(\gamma_t, \lambda_0, \tilde{C}_L, C_{D,p}, AR, \kappa_0, \xi_t) \right) \quad (38)$$

subject to: $h(\gamma_t, \lambda_0, \tilde{C}_L, C_{D,p}, AR, \kappa_0) = 0$.

In Fig. 8, the analytical solution (Eq. 36) is compared with the optimization problems results. For $\kappa_0 = 0$, the optimal AR for Ground-Gen is equal to the analytical expression, while for Fly-Gen is slightly different because Eq. (36) is derived by considering thrust power and not shaft power. By increasing κ_0 , the optimal aspect ratio increases of by a relatively small value compared to the analytical solution. Equation (36) can then be used in design and optimization studies as an educated initial guess for the wing aspect ratio, when the design wing lift coefficient and the parasite drag coefficient at zero lift are known.

In the last study of this section, the optimal power coefficient is studied as function of the design lift coefficient for different inverse turning ratios. By using the analytical expression for the optimal AR (Eq. 36), obtained with $C_{Di}^n = C_{D,p}$, into Eqs. 300 (20) and (29) (the thrust power coefficient for Fly-Gen is considered), the maximum power coefficient C_P^\otimes with straight wake

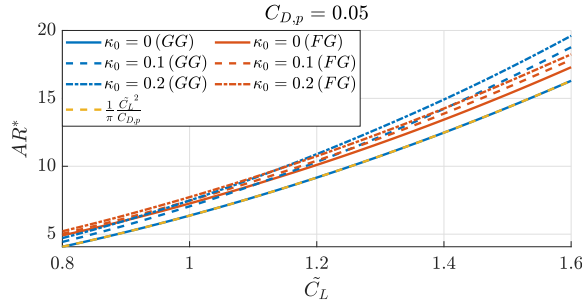


Figure 8. Optimal aspect ratio found analytically AR^\otimes and numerically AR^* for Ground-Gen (blue lines) and Fly-Gen (red lines) for different κ_0 as function of the design lift coefficient \tilde{C}_L . Case with $C_{D,p} = 0.05$ and $\xi_t = 0.15$.

($\kappa_0 = 0$) is

$$C_P^\otimes = \frac{1}{27} \frac{\tilde{C}_L}{C_{D,p}}. \quad (39)$$

This power coefficient physically represents the upper bound of the power production of an AWES flying in a circular path with infinite radius, for given design lift coefficient and parasite drag coefficient. [at zero lift](#).

305 [With Following](#) a similar procedure, a corresponding thrust coefficient is found by inserting the analytical expression for AR^\otimes into Eq. (18) with $\gamma_o = 1/3$ and Eq. (31) with $\gamma_t = 1/2$ and considering $\kappa_0 = 0$

$$C_T^\otimes = \frac{1}{9} \frac{\tilde{C}_L}{C_{D,p}}. \quad (40)$$

Figure 9 shows the optimal power coefficients, found by solving the optimization problems (37) and (38), as function of \tilde{C}_L for different κ_0 . The maximum power coefficient, considering straight wakes, of Fly-Gen AWESs is slightly lower than the analytical maximum power coefficient C_P^\otimes (Eq. 39) and than $C_{P,GG}^*(\kappa_0 = 0)$ because of the power losses due to onboard wind turbine induction. For increasing κ_0 , the maximum power coefficient decreases. As noted when analyzing Fig. 7, Fly-Gen have a higher power generation potential compared to Ground-Gen AWESs. The power coefficients of Ground-Gen (Eq. 17, [blue lines](#)) and Fly-Gen (Eq. 30, [red lines](#)) are defined taking the disc with radius equal to the AWES wing span as reference area. Considering this reference area, the AWES power coefficient can take values higher than the Betz limit and the unity without violating any physical law. Note that the power coefficient for Ground-Gen AWESs neglects the reel-in phase and the losses due to the potential energy exchange, while the power coefficient for Fly-Gen AWESs neglects the losses due to the potential energy exchange.

315

In this section, Ground-Gen and Fly-Gen AWESs, with the same geometry, are compared. Fly-Gen AWESs have smaller glide ratios because the on-board wind turbines thrust is included in the drag estimation. Ground-Gen AWESs fly closer to their own wake due to the reel-out velocity, thus having a larger normalized torsional parameter λ_0 . Fly-Gen AWESs can then harvest more power because of the wake structure. If the aspect ratio is increased, higher power coefficients can be obtained at high operational lift coefficients. The aspect ratio which maximizes the power coefficient is finite and the analytical solution

320

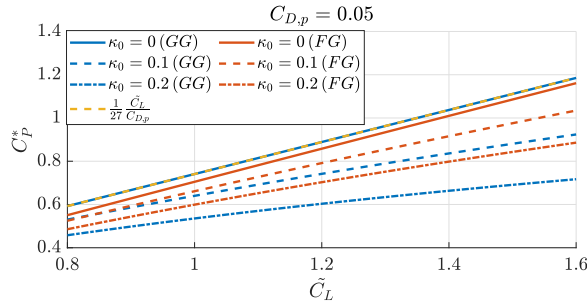


Figure 9. Aerodynamic power coefficients, as function of the design lift coefficient \tilde{C}_L , of Ground-Gen (blue lines) and Fly-Gen (red lines) AWESs and maximum aerodynamic power coefficient (yellow dashed line). Case with $C_{D,p} = 0.05$, $\xi_t = 0.15$, the optimal aspect ratios AR^* and the optimal coefficients $\gamma_o = 1/3$ and γ_t^* .

for straight wakes is $\frac{1}{\pi} \frac{\tilde{C}_L^2}{C_{D,p}}$. This analytical expression can be used in the preliminary design phase of an AWES project. By considering the optimal aspect ratio, the maximum thrust and power coefficients can be found and their analytical expressions for straight wakes obtained. The expression for the maximum power coefficient $C_P^\otimes = \frac{1}{27} \frac{\tilde{C}_L}{C_{D,p}}$ can be used to estimate the upper bound of an AWES power production.

6 Numerical examples

In this section, three AWESs two Ground-Gen and one Fly-Gen AWESs from the literature are analyzed based on the mathematical models introduced in this paper. In particular, the inverse turning ratio, the glide ratio, the contribution from the far wake induced drag coefficient and the power coefficients are analyzed.

In Table 1, the parameters describing two Ground-Gen the selected AWESs are given. Zefiro is an ultralight glider, its flight mechanics, when used as a Ground-Gen AWES, is studied by Trevisi et al. (2021) and its design by Trevisi et al. (2022b). MegAWES refers to the AWES introduced by Eijkelhof and Schmehl (2022). As Zefiro and MegAWES operate at different tether length during the reel-out phase, they are studied at the initial and the final tether length. In Table 2, the parameters describing the Makani MX2 design, which is the Fly-Gen AWES chosen for the example, are given. The Makani MX2 (Tucker (2020)) is a Fly-Gen AWES, a detailed analysis of the its power losses due to potential energy exchange of the MX2 is carried out by Trevisi et al. (2022a).

To start the analysis, the optimal onboard wind turbine thrust factor γ_t^* (blue - left axis) and the relative efficiency due to the onboard wind turbine induction (red - right axis) for the MX2 are shown in Fig. 10. The MX2 is designed to operate at a lift coefficient of $C_L = 1.8$, leading to an efficiency of $1 - a_t \approx 96.5\%$ in steady state. Even if the power losses due to the onboard wind turbine induction seem small in steady state, they are responsible for modifying the optimal trajectories at low wind speed and reducing the power production, as shown by Trevisi et al. (2022a).

Table 1. Reference values for the Ground-Gen AWESs examples Reference values for the examples. Zefiro (Trevisi et al. (2022b)) and MegAWES (Eijkelhof and Schmehl (2022)) are Ground-Gen AWESs, the Makani MX2 is a Fly-Gen AWES (Tucker (2020)).

Zefiro	m	530 kg	A	14.25 m²	b	15.18 m	AR	16.2	C_d	0.018	$C_{D\perp}$	0.8
	D_t	0.01	$L_{t,in}$	100 m	$C_{D,p,in}$	0.032	$L_{t,fin}$	700 m	$C_{D,p,fin}$	0.116		
MegAWES	m	6885 kg	A	150 m²	b	42.5 m	AR	12	C_d	0.02	$C_{D\perp}$	1.2
	D_t	0.03	$L_{t,in}$	750 m	$C_{D,p,in}$	0.065	$L_{t,fin}$	1500 m	$C_{D,p,fin}$	0.110		
MX2	m	2000 kg	b	26 m	AR	12.5	C_d	0.04	$C_{D\perp}$	0.7		
	D_t	0.03	L_t	300 m	$C_{D,p}$	0.069	A_t	35 m ²	ξ_t	0.18		

Table 2. Reference values for the examples (Values from the Makani MX2 description-Tucker (2020)).

MX2	m	2000 kg	A	54 m²	b	26 m	AR	12.5	C_d	0.04	$C_{D\perp}$	0.7
	D_t	0.03	L_t	300 m	$C_{D,p}$	0.069	A_t	35 m ²	ξ_t	0.18		

In Fig. 11, the inverse turning ratios are shown as function of the lift coefficient. The optimal opening angle Φ , computed with Eq. (15), is used to find the turning radius R_0 and thus $\kappa_0 = \frac{b/2}{R_0}$. The inverse turning ratio is larger for Ground-Gen
 345 AWESs at the initial tether length. Note that the vortex model assumes a fully developed wake and this assumption does not hold when analyzing the first few loops of the reel-out phase.

In Fig. 12, the glide ratio is shown. As noted when comparing Ground-Gen and Fly-Gen AWESs in Sect. 5, the Fly-Gen MX2 has lower glide ratio as the onboard wind turbine thrust is included in the drag estimation. The tether length is largely influencing the glide ratio. At low tether length, the glide ratio is higher because the tether drag contributes with a small share
 350 to the **parasite** drag coefficient **at zero lift** $C_{D,p}$.

In Fig. 13, the ratio of induced drag due to the far wake to the total induced drag is shown. For Ground-Gen AWESs, the far wake contribution is high at low tether length and decreases during the reel-out, as the inverse turning ratio (Fig. 11) and the glide ratio (Fig. 12) decrease.

Finally, the optimal power coefficients are shown in Fig. 14. Ground-Gen AWESs at low tether lengths can achieve higher
 355 optimal C_P . ~~Note that Zefiro, at the initial tether length, maximizes power with a lift coefficient of approximately $C_L \approx 1.5$~~ At the initial tether length, Zefiro maximizes power with a lift coefficient of approximately $C_L \approx 1.5$ and MegAWEs of approximately $C_L \approx 2$. This indicates that, from aerodynamic considerations, operating the AWES at different lift coefficients could be optimal at different tether length. The MX2 maximizes power with a lift coefficient of approximately $C_L \approx 2.3$. This shows that higher lift coefficients could be not required for a design similar to the MX2.

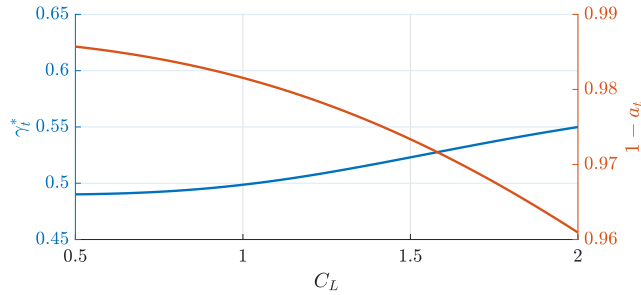


Figure 10. Optimal value of γ_t (blue—left axis) and efficiency due to onboard wind turbine induction (red—right axis) as function of the lift coefficient for the MX2 design (Table 2).

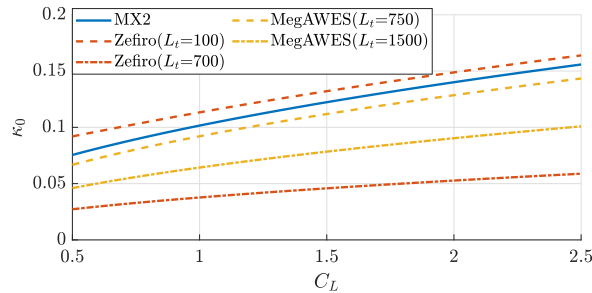


Figure 11. Inverse turning ratios as function of the lift coefficient for the examples (Tables 1 and 2). Ground-Gen AWESs κ_0 is shown at initial and final tether length.

360 7 Conclusions

In this work, the aerodynamic wake model developed by Trevisi et al. (2023b) is used to refine the power equations of Ground-Gen and Fly-Gen AWESs. The aerodynamic model assumes steady crosswind circular trajectories and a non-expanding heli-
 coidal vortex wake. The main assumptions and equations of the wake model are reported in Sect. 2. The power equations of
 Ground-Gen and Fly-Gen AWESs are refined by accounting for the aerodynamic wake in the induced drag coefficient estima-
 365 tion. In this way, the effects of changing geometrical and aerodynamic quantities aspect ratio, turning radius, lift coefficient,
 parasite drag coefficient, dimension of the onboard turbines (for Fly-Gen AWESs) and control quantities (reel-out velocity
 for Ground-Gen and on-board wind turbine thrust for Fly-Gen AWESs) on the overall aerodynamic performances and on the
 power production can be intuitively understood. For Ground-Gen AWESs, the optimal reel-out velocity is not influenced by the
 wake structure. For Fly-Gen AWESs, the onboard wind turbines induction is modelled with 1D momentum theory, such that
 370 the power at the onboard turbine shaft is found. The optimal onboard wind turbines thrust, for Fly-Gen, is slightly influenced
 by the wake structure, while the optimal reel-out velocity, for Ground-Gen, is not.

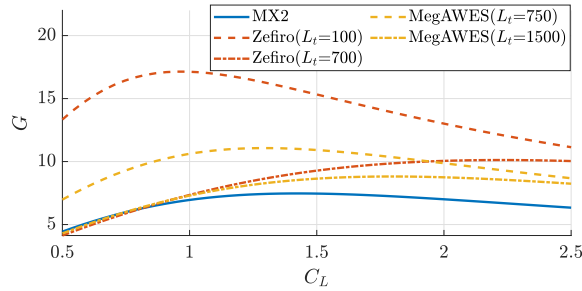


Figure 12. Glide ratios as function of the lift coefficient for the examples (Tables 1 and 2). Ground-Gen AWESs G is shown at initial and final tether length.

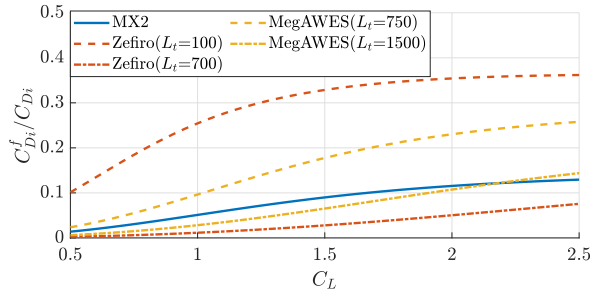


Figure 13. Ratio between the induced drag due to the far wake and the total induced drag as function of the lift coefficient for the examples (Tables 1 and 2). Ground-Gen AWESs values are shown at initial and final tether length.

To compare different concepts, A novel power coefficient is defined by normalizing the aerodynamic power with the wind power passing through a disc with radius equal to the AWES wing span, allowing to compare different designs for a given wing span. The aspect ratio which maximizes this power coefficient (i.e. which maximizes the aerodynamic power for a given wing span) is found to be finite. Considering an infinite turning radius, the optimal aspect ratio, considering an infinite turning radius, is $\frac{1}{\pi} \frac{\tilde{C}_L^2}{C_{D,p}}$, where \tilde{C}_L is the design lift coefficient and $C_{D,p}$ the parasite drag coefficient at zero lift. For decreasing turning radii, the optimal aspect ratios slightly increase with respect to the analytical expression. Considering an infinite turning radius and the optimal aspect ratio, and the maximum power coefficient is $\frac{1}{27} \frac{\tilde{C}_L}{C_{D,p}}$. For decreasing turning radii, the maximum power coefficients decrease with respect to the analytical expression. For decreasing turning radii, the optimal aspect ratios slightly increase and the maximum power coefficients decrease with respect to the analytical expressions.

By comparing power coefficients, Ground-Gen AWESs are found to have lower power generation potential compared with respect to the same geometry Fly-Gen AWESs with the same geometry because they fly closer to their own wake, due to the reel-out velocity of the tether. To conclude, Three AWESs of different sizes from the literature are studied. The Two Ground-Gen AWESs are analyzed at the initial and final tether length of the reel-out phase, finding that higher power coefficients can

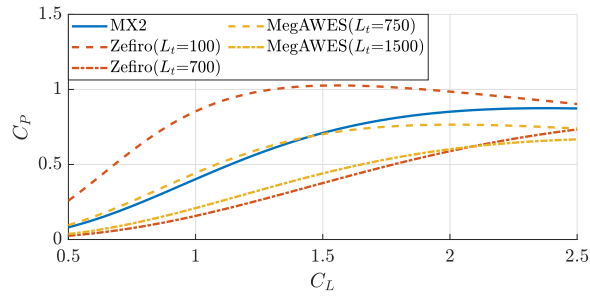


Figure 14. Optimal Power coefficients as function of the lift coefficient for the examples (Tables 1 and 2). Ground-Gen AWESs C_P is shown at initial and final tether length.

385 be obtained at shorter tether length because of the reduced tether drag. A Fly-Gen AWES is analyzed, finding that power is maximized at a finite lift coefficient.

Appendix A: Nomenclature

Latin symbols

A	Wing area
AR	Wing aspect ratio
b	Wing span
C_d	Wing profile drag coefficient
C_D	System drag coefficient
$C_{D,c}$	Drag coefficient modelling all AWES components excluding the main wing and the tether
C_{D_i}	Induced drag coefficient
$C_{D_i}^f$	Induced drag coefficient due to the far wake
$C_{D_i}^m$	Induced drag coefficient due to the near wake
$C_{D,p}$	Parasite drag coefficient
$C_{D\perp}$	Drag coefficient of the tether section
$C_{D,t}$	Equivalent tether drag coefficient
C_L	Wing lift coefficient
\tilde{C}_L	Design wing lift coefficient
C_P	Power coefficient
C_{Pt}	Thrust power coefficient (for Fly-Gen AWESs)
C_T	Thrust coefficient
$C_{T,t}$	On-board wind turbine thrust coefficient with respect to the AWES wing area
D_t	Tether diameter
G	$C_L / (C_D + C_{T,t})$: Glide ratio
h_0	Helicoidal wake pitch
L_t	Tether length
m	AWES mass plus one third of the tether mass
R_0	Mid-span turning radius
u_0	AWES longitudinal velocity
v_a	Apparent wind speed
v_r	Relative wind speed
v_w	Wind speed

Greek symbols

γ_o	v_o/v_w : reel-out factor
γ_t	$C_{T,t}/C_D$: on-board wind turbine thrust factor
κ_0	$b/(2R_0)$: inverse turning ratio
λ	u_0/v_r : wing speed ratio
λ_0	Normalized torsional parameter of the helicoidal wake
Φ	Opening angle of the cone swept by the AWESs during one loop
ρ	Air density

Symbols

- * Optimal quantity
- ⊗ Optimal quantity found analytically

Code and data availability. All figures and the MATLAB code developed to generate them can be retried via <https://doi.org/10.5281/zenodo.8210953> (Trevisi et al. (2023a)). The figures can be opened with MATLAB or other open-source programming languages (e.g., Python, Octave).

Author contributions. FT conceptualized and developed the research methods, produced the results and wrote the draft version of the paper. AC and CEDR supervised the research, supported the methodology conceptualization and reviewed the paper.

Competing interests. Alessandro Croce is a member of the editorial board of Wind Energy Science. The authors have no other competing interests to declare.

Acknowledgements. This work has been partially supported by the MERIDIONAL project, which receives funding from the European Union's Horizon Europe Programme under the grant agreement No. 101084216

References

- Anderson, J.: *Fundamentals of Aerodynamics*, McGraw-Hill Education, sixth edn., <http://lccn.loc.gov/2015040997>, 2017.
- Argatov, I. and Silvennoinen, R.: Efficiency of Traction Power Conversion Based on Crosswind Motion, in: *Airborne Wind Energy*, edited by Ahrens, U., Diehl, M., and Schmehl, R., pp. 65–79, Springer Berlin Heidelberg, Berlin, Heidelberg, https://doi.org/10.1007/978-3-642-39965-7_4, 2013.
- Bauer, F., Kennel, R. M., Hackl, C. M., Campagnolo, F., Patt, M., and Schmehl, R.: Drag power kite with very high lift coefficient, *Renewable Energy*, 118, 290–305, <https://doi.org/10.1016/j.renene.2017.10.073>, 2018.
- De Lellis, M., Reginatto, R., Saraiva, R., and Trofino, A.: The Betz limit applied to Airborne Wind Energy, *Renewable Energy*, 127, 32–40, <https://doi.org/10.1016/j.renene.2018.04.034>, 2018.
- Diehl, M.: *Airborne Wind Energy: Basic Concepts and Physical Foundations*, in: *Airborne Wind Energy*, edited by Ahrens, U., Diehl, M., and Schmehl, R., pp. 3–22, Springer Berlin Heidelberg, Berlin, Heidelberg, https://doi.org/10.1007/978-3-642-39965-7_1, 2013.
- Eijkelhof, D. and Schmehl, R.: Six-degrees-of-freedom simulation model for future multi-megawatt airborne wind energy systems, *Renewable Energy*, 196, 137–150, <https://doi.org/10.1016/j.renene.2022.06.094>, 2022.
- 410 Gaunaa, M., Forsting, A. M., and Trevisi, F.: An engineering model for the induction of crosswind kite power systems, *Journal of Physics: Conference Series*, 1618, 032010, <https://doi.org/10.1088/1742-6596/1618/3/032010>, 2020.
- Kheiri, M., Bourgault, F., Saberi Nasrabad, V., and Victor, S.: On the aerodynamic performance of crosswind kite power systems, *Journal of Wind Engineering and Industrial Aerodynamics*, 181, 1–13, <https://doi.org/10.1016/j.jweia.2018.08.006>, 2018.
- Kheiri, M., Saberi Nasrabad, V., and Bourgault, F.: A new perspective on the aerodynamic performance and power limit of crosswind kite systems, *Journal of Wind Engineering and Industrial Aerodynamics*, 190, 190–199, <https://doi.org/10.1016/j.jweia.2019.04.010>, 2019.
- 415 Leuthold, R., Crawford, C., Gros, S., and Diehl, M.: Engineering Wake Induction Model For Axisymmetric Multi-Kite Systems, *Journal of Physics: Conference Series*, <https://doi.org/10.1088/1742-6596/1256/1/012009>, 2019.
- Loyd, M.: Crosswind Kite Power, *Journal of Energy*, 4, 106–111, 1980.
- Luchsinger, R. H.: Pumping Cycle Kite Power, in: *Airborne Wind Energy*, edited by Ahrens, U., Diehl, M., and Schmehl, R., pp. 47–64, https://doi.org/10.1007/978-3-642-39965-7_3, 2013.
- 420 Marten, D., Lennie, M., Pechlivanoglou, G., Nayeri, C. N., and Paschereit, C. O.: Implementation, Optimization and Validation of a Non-linear Lifting Line Free Vortex Wake Module Within the Wind Turbine Simulation Code QBlade, Volume 9: Oil and Gas Applications; Supercritical CO2 Power Cycles; *Wind Energy*, <https://doi.org/10.1115/GT2015-43265>, 2015.
- Schmehl, R., Noom, M., and van der Vlugt, R.: Traction Power Generation with Tethered Wings, in: *Airborne Wind Energy*, edited by Ahrens, U., Diehl, M., and Schmehl, R., pp. 23–45, Springer Berlin Heidelberg, Berlin, Heidelberg, https://doi.org/10.1007/978-3-642-39965-7_2, 2013.
- 425 Trevisi, F., Gaunaa, M., and McWilliam, M.: The Influence of Tether Sag on Airborne Wind Energy Generation., *Journal of Physics: Conference Series*, 1618, <https://doi.org/10.1088/1742-6596/1618/3/032006>, 2020a.
- Trevisi, F., Gaunaa, M., and McWilliam, M.: Unified engineering models for the performance and cost of Ground-Gen and Fly-Gen crosswind Airborne Wind Energy Systems, *Renewable Energy*, 162, 893–907, <https://doi.org/10.1016/j.renene.2020.07.129>, 2020b.
- 430 Trevisi, F., Croce, A., and Riboldi, C. E. D.: Flight Stability of Rigid Wing Airborne Wind Energy Systems, *Energies*, 14, <https://doi.org/10.3390/en14227704>, 2021.

- Trevisi, F., Castro-Fernández, I., Pasquinelli, G., Riboldi, C. E. D., and Croce, A.: Flight trajectory optimization of Fly-Gen airborne wind energy systems through a harmonic balance method, *Wind Energy Science*, 7, 2039–2058, <https://doi.org/10.5194/wes-7-2039-2022>, 435 2022a.
- Trevisi, F., Riboldi, C. E. D., and Croce, A.: Sensitivity analysis of a Ground-Gen Airborne Wind Energy System design., *Journal of Physics: Conference Series*, 2265, 042 067, <https://doi.org/10.1088/1742-6596/2265/4/042067>, 2022b.
- Trevisi, F., Riboldi, C. E. D., and Croce, A.: Figures and code: Refining the airborne wind energy systems power equations with a vortex wake model, <https://doi.org/10.5281/zenodo.8210953>, 2023a.
- 440 Trevisi, F., Riboldi, C. E. D., and Croce, A.: Vortex model of the aerodynamic wake of airborne wind energy systems, *Wind Energy Science*, 8, 999–1016, <https://doi.org/10.5194/wes-8-999-2023>, 2023b.
- Tucker, N.: Airborne Wind Turbine Performance: Key Lessons From More Than a Decade of Flying Kites., in: *The Energy Kite Part I.*, edited by Echeverri, P., Fricke, T., Homsy, G., and Tucker, N., pp. 93–224, <https://x.company/projects/makani/#>, 2020.
- Vander Lind, D.: Analysis and Flight Test Validation of High Performance Airborne Wind Turbines, in: *Airborne Wind Energy*, edited by 445 Ahrens, U., Diehl, M., and Schmehl, R., pp. 473–490, Springer Berlin Heidelberg, Berlin, Heidelberg, https://doi.org/10.1007/978-3-642-39965-7_28, 2013.
- Vermillion, C., Cobb, M., Fagiano, L., Leuthold, R., Diehl, M., Smith, R. S., Wood, T. A., Rapp, S., Schmehl, R., Olinger, D., and Demetriou, M.: Electricity in the air: Insights from two decades of advanced control research and experimental flight testing of airborne wind energy systems, *Annual Reviews in Control*, 52, 330–357, <https://doi.org/10.1016/j.arcontrol.2021.03.002>, 2021.